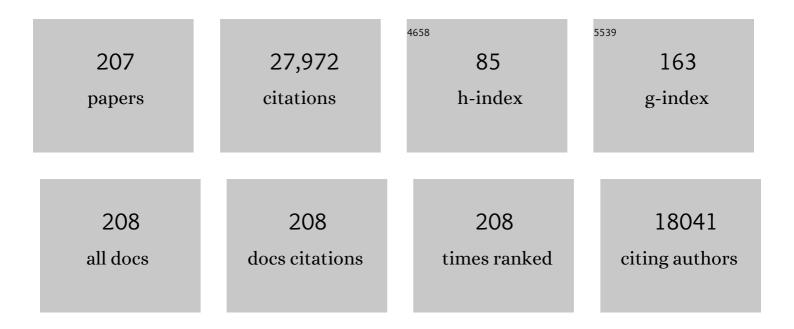
List of Publications by Year in descending order

Source: https://exaly.com/author-pdf/5670671/publications.pdf Version: 2024-02-01



#	Article	IF	CITATIONS
1	Efficient Visible Light Nitrogen Fixation with BiOBr Nanosheets of Oxygen Vacancies on the Exposed {001} Facets. Journal of the American Chemical Society, 2015, 137, 6393-6399.	13.7	1,468
2	Synthesis and Facet-Dependent Photoreactivity of BiOCl Single-Crystalline Nanosheets. Journal of the American Chemical Society, 2012, 134, 4473-4476.	13.7	1,326
3	Generalized One-Pot Synthesis, Characterization, and Photocatalytic Activity of Hierarchical BiOX (X) Tj ETQq1 1	0.784314 3.1	rgBT /Ove
4	Oxygen Vacancyâ€Mediated Photocatalysis of BiOCl: Reactivity, Selectivity, and Perspectives. Angewandte Chemie - International Edition, 2018, 57, 122-138.	13.8	871
5	Bismuth oxyhalide nanomaterials: layered structures meet photocatalysis. Nanoscale, 2014, 6, 8473-8488.	5.6	774
6	New Reaction Pathway Induced by Plasmon for Selective Benzyl Alcohol Oxidation on BiOCl Possessing Oxygen Vacancies. Journal of the American Chemical Society, 2017, 139, 3513-3521.	13.7	693
7	Low-Temperature Synthesis and High Visible-Light-Induced Photocatalytic Activity of BiOI/TiO ₂ Heterostructures. Journal of Physical Chemistry C, 2009, 113, 7371-7378.	3.1	633
8	Surface Structure-Dependent Molecular Oxygen Activation of BiOCl Single-Crystalline Nanosheets. Journal of the American Chemical Society, 2013, 135, 15750-15753.	13.7	560
9	Solar Water Splitting and Nitrogen Fixation with Layered Bismuth Oxyhalides. Accounts of Chemical Research, 2017, 50, 112-121.	15.6	554
10	Efficient Ammonia Electrosynthesis from Nitrate on Strained Ruthenium Nanoclusters. Journal of the American Chemical Society, 2020, 142, 7036-7046.	13.7	542
11	ZnO/BiOI Heterostructures: Photoinduced Charge-Transfer Property and Enhanced Visible-Light Photocatalytic Activity. Journal of Physical Chemistry C, 2011, 115, 20555-20564.	3.1	539
12	Giant Enhancement of Internal Electric Field Boosting Bulk Charge Separation for Photocatalysis. Advanced Materials, 2016, 28, 4059-4064.	21.0	538
13	Porous structure dependent photoreactivity of graphitic carbon nitride under visible light. Journal of Materials Chemistry, 2012, 22, 1160-1166.	6.7	446
14	Efficient Photocatalytic Removal of NO in Indoor Air with Hierarchical Bismuth Oxybromide Nanoplate Microspheres under Visible Light. Environmental Science & Technology, 2009, 43, 4143-4150.	10.0	426
15	Superior visible light hydrogen evolution of Janus bilayer junctions via atomic-level charge flow steering. Nature Communications, 2016, 7, 11480.	12.8	403
16	Oxygen Vacancy Associated Surface Fenton Chemistry: Surface Structure Dependent Hydroxyl Radicals Generation and Substrate Dependent Reactivity. Environmental Science & Technology, 2017, 51, 5685-5694.	10.0	387
17	Hydroxylamine Promoted Goethite Surface Fenton Degradation of Organic Pollutants. Environmental Science & Technology, 2017, 51, 5118-5126.	10.0	370
18	Highly efficient photocatalytic removal of sodium pentachlorophenate with Bi3O4Br under visible light. Applied Catalysis B: Environmental, 2013, 136-137, 112-121.	20.2	338

#	Article	IF	CITATIONS
19	Sustainable molecular oxygen activation with oxygen vacancies on the {001} facets of BiOCl nanosheets under solar light. Nanoscale, 2014, 6, 14168-14173.	5.6	334
20	Oxygen Vacancy Structure Associated Photocatalytic Water Oxidation of BiOCl. ACS Catalysis, 2016, 6, 8276-8285.	11.2	333
21	Oxygen Vacancy Promoted O ₂ Activation over Perovskite Oxide for Low-Temperature CO Oxidation. ACS Catalysis, 2019, 9, 9751-9763.	11.2	296
22	Efficient Removal of Cr(VI) from Aqueous Solution with Fe@Fe ₂ O ₃ Coreâ^'Shell Nanowires. Environmental Science & Technology, 2008, 42, 6955-6960.	10.0	283
23	Protocatechuic Acid Promoted Alachlor Degradation in Fe(III)/H ₂ O ₂ Fenton System. Environmental Science & Technology, 2015, 49, 7948-7956.	10.0	278
24	Core–Shell Structure Dependent Reactivity of Fe@Fe ₂ O ₃ Nanowires on Aerobic Degradation of 4-Chlorophenol. Environmental Science & Technology, 2013, 47, 5344-5352.	10.0	272
25	Selective oxidation of benzyl alcohol into benzaldehyde over semiconductors under visible light: The case of Bi12O17Cl2 nanobelts. Applied Catalysis B: Environmental, 2013, 142-143, 487-493.	20.2	268
26	Visible Light Photocatalysis of BiOI and Its Photocatalytic Activity Enhancement by in Situ Ionic Liquid Modification. Journal of Physical Chemistry C, 2011, 115, 14300-14308.	3.1	267
27	Persistent free radicals in carbon-based materials on transformation of refractory organic contaminants (ROCs) in water: A critical review. Water Research, 2018, 137, 130-143.	11.3	255
28	Facet-Dependent Cr(VI) Adsorption of Hematite Nanocrystals. Environmental Science & Technology, 2016, 50, 1964-1972.	10.0	246
29	Facet-dependent solar ammonia synthesis of BiOCl nanosheets via a proton-assisted electron transfer pathway. Nanoscale, 2016, 8, 1986-1993.	5.6	242
30	Enhanced Photocatalytic Removal of Sodium Pentachlorophenate with Self-Doped Bi ₂ WO ₆ under Visible Light by Generating More Superoxide Ions. Environmental Science & Technology, 2014, 48, 5823-5831.	10.0	239
31	Visible light driven selective oxidation of amines to imines with BiOCI: Does oxygen vacancy concentration matter?. Applied Catalysis B: Environmental, 2018, 228, 87-96.	20.2	237
32	Self-doping and surface plasmon modification induced visible light photocatalysis of BiOCl. Nanoscale, 2013, 5, 10573.	5.6	233
33	Iron oxide shell mediated environmental remediation properties of nano zero-valent iron. Environmental Science: Nano, 2017, 4, 27-45.	4.3	219
34	Oxygen Vacancies Promoted the Selective Photocatalytic Removal of NO with Blue TiO ₂ via Simultaneous Molecular Oxygen Activation and Photogenerated Hole Annihilation. Environmental Science & Technology, 2019, 53, 6444-6453.	10.0	215
35	Fe@Fe2O3 core-shell nanowires enhanced Fenton oxidation by accelerating the Fe(III)/Fe(II) cycles. Water Research, 2014, 59, 145-153.	11.3	211
36	Photochemistry of Hydrochar: Reactive Oxygen Species Generation and Sulfadimidine Degradation. Environmental Science & Technology, 2017, 51, 11278-11287.	10.0	208

#	Article	IF	CITATIONS
37	Electronic and Band Structure Tuning of Ternary Semiconductor Photocatalysts by Self Doping: The Case of BiOI. Journal of Physical Chemistry C, 2010, 114, 18198-18206.	3.1	201
38	Hydrothermal Synthesis of FeS ₂ as a High-Efficiency Fenton Reagent to Degrade Alachlor via Superoxide-Mediated Fe(II)/Fe(III) Cycle. ACS Applied Materials & Interfaces, 2015, 7, 28534-28544.	8.0	193
39	Spin-State-Dependent Peroxymonosulfate Activation of Single-Atom M–N Moieties via a Radical-Free Pathway. ACS Catalysis, 2021, 11, 9569-9577.	11.2	192
40	Ascorbic acid/Fe@Fe2O3: A highly efficient combined Fenton reagent to remove organic contaminants. Journal of Hazardous Materials, 2016, 310, 170-178.	12.4	189
41	Efficient Removal of Heavy Metal Ions with Biopolymer Template Synthesized Mesoporous Titania Beads of Hundreds of Micrometers Size. Environmental Science & Technology, 2012, 46, 419-425.	10.0	185
42	Synthesis and internal electric field dependent photoreactivity of Bi ₃ O ₄ Cl single-crystalline nanosheets with high {001} facet exposure percentages. Nanoscale, 2014, 6, 167-171.	5.6	185
43	Nonaqueous Solâ~'Gel Synthesized Hierarchical CeO ₂ Nanocrystal Microspheres as Novel Adsorbents for Wastewater Treatment. Journal of Physical Chemistry C, 2009, 113, 16625-16630.	3.1	178
44	Oxygen vacancy induced selective silver deposition on the {001} facets of BiOCl single-crystalline nanosheets for enhanced Cr(<scp>vi</scp>) and sodium pentachlorophenate removal under visible light. Nanoscale, 2014, 6, 7805-7810.	5.6	173
45	Hydrothermal Carbon-Mediated Fenton-Like Reaction Mechanism in the Degradation of Alachlor: Direct Electron Transfer from Hydrothermal Carbon to Fe(III). ACS Applied Materials & Interfaces, 2017, 9, 17115-17124.	8.0	163
46	Dramatically Enhanced Aerobic Atrazine Degradation with Fe@Fe ₂ O ₃ Core–Shell Nanowires by Tetrapolyphosphate. Environmental Science & Technology, 2014, 48, 3354-3362.	10.0	158
47	Self doping promoted photocatalytic removal of no under visible light with bi2moo6: Indispensable role of superoxide ions. Applied Catalysis B: Environmental, 2016, 182, 316-325.	20.2	157
48	Facile Microwave-Assisted Synthesis and Magnetic and Gas Sensing Properties of Fe ₃ O ₄ Nanoroses. Journal of Physical Chemistry C, 2010, 114, 6237-6242.	3.1	152
49	Efficient anoxic pollutant removal with oxygen functionalized graphitic carbon nitride under visible light. RSC Advances, 2014, 4, 5553.	3.6	152
50	Simultaneous Manipulation of Bulk Excitons and Surface Defects for Ultrastable and Highly Selective CO ₂ Photoreduction. Advanced Materials, 2021, 33, e2100143.	21.0	151
51	Van Der Waals gap-rich BiOCl atomic layers realizing efficient, pure-water CO2-to-CO photocatalysis. Nature Communications, 2021, 12, 5923.	12.8	150
52	Fe@Fe2O3 Coreâ~'Shell Nanowires as Iron Reagent. 1. Efficient Degradation of Rhodamine B by a Novel Sono-Fenton Process. Journal of Physical Chemistry C, 2007, 111, 4087-4093.	3.1	149
53	Oxygen Vacancies Mediated Complete Visible Light NO Oxidation via Side-On Bridging Superoxide Radicals. Environmental Science & Technology, 2018, 52, 8659-8665.	10.0	149
54	Liquid Nitrogen Activation of Zero-Valent Iron and Its Enhanced Cr(VI) Removal Performance. Environmental Science & Technology, 2019, 53, 8333-8341.	10.0	149

#	Article	IF	CITATIONS
55	Facetâ€Level Mechanistic Insights into General Homogeneous Carbon Doping for Enhanced Solarâ€toâ€Hydrogen Conversion. Advanced Functional Materials, 2015, 25, 2189-2201.	14.9	146
56	Synthesis and Characterization of Feâ^'Fe2O3Coreâ^'Shell Nanowires and Nanonecklaces. Crystal Growth and Design, 2007, 7, 459-464.	3.0	143
57	Phosphate Shifted Oxygen Reduction Pathway on Fe@Fe ₂ O ₃ Core–Shell Nanowires for Enhanced Reactive Oxygen Species Generation and Aerobic 4-Chlorophenol Degradation. Environmental Science & Technology, 2017, 51, 8101-8109.	10.0	143
58	Electrochemically self-doped WO3/TiO2 nanotubes for photocatalytic degradation of volatile organic compounds. Applied Catalysis B: Environmental, 2020, 260, 118205.	20.2	142
59	Generalized Preparation of Porous Nanocrystalline ZnFe ₂ O ₄ Superstructures from Zinc Ferrioxalate Precursor and Its Superparamagnetic Property. Journal of Physical Chemistry C, 2008, 112, 13163-13170.	3.1	138
60	In Situ Carbon Homogeneous Doping on Ultrathin Bismuth Molybdate: A Dualâ€Purpose Strategy for Efficient Molecular Oxygen Activation. Advanced Functional Materials, 2017, 27, 1703923.	14.9	136
61	Insight into Core–Shell Dependent Anoxic Cr(VI) Removal with Fe@Fe ₂ O ₃ Nanowires: Indispensable Role of Surface Bound Fe(II). ACS Applied Materials & Interfaces, 2015, 7, 1997-2005.	8.0	134
62	Design of a Highly Efficient and Wide pH Electro-Fenton Oxidation System with Molecular Oxygen Activated by Ferrous–Tetrapolyphosphate Complex. Environmental Science & Technology, 2015, 49, 3032-3039.	10.0	132
63	Synthesis and Enhanced Cr(VI) Photoreduction Property of Formate Anion Containing Graphitic Carbon Nitride. Journal of Physical Chemistry C, 2013, 117, 4062-4068.	3.1	127
64	Hematite facet confined ferrous ions as high efficient Fenton catalysts to degrade organic contaminants by lowering H2O2 decomposition energetic span. Applied Catalysis B: Environmental, 2016, 181, 127-137.	20.2	127
65	Direct Oxidation of Methanol on Self-Supported Nanoporous Gold Film Electrodes with High Catalytic Activity and Stability. Chemistry of Materials, 2007, 19, 6065-6067.	6.7	123
66	Energy-confined solar thermal ammonia synthesis with K/Ru/TiO2-xHx. Applied Catalysis B: Environmental, 2018, 224, 612-620.	20.2	122
67	Anion (O, N, C, and S) vacancies promoted photocatalytic nitrogen fixation. Green Chemistry, 2019, 21, 2852-2867.	9.0	121
68	Ascorbate-Promoted Surface Iron Cycle for Efficient Heterogeneous Fenton Alachlor Degradation with Hematite Nanocrystals. ACS Applied Materials & amp; Interfaces, 2017, 9, 8751-8758.	8.0	120
69	Total aerobic destruction of azo contaminants with nanoscale zero-valent copper at neutral pH: Promotion effect of in-situ generated carbon center radicals. Water Research, 2014, 66, 22-30.	11.3	118
70	First observation of visible light photocatalytic activity of carbon modified Nb2O5 nanostructures. Journal of Materials Chemistry, 2010, 20, 3052.	6.7	117
71	A highly efficient zinc catalyst for selective electroreduction of carbon dioxide in aqueous NaCl solution. Journal of Materials Chemistry A, 2015, 3, 16409-16413.	10.3	117
72	Adjacent single-atom irons boosting molecular oxygen activation on MnO2. Nature Communications, 2021, 12, 5422.	12.8	114

#	Article	IF	CITATIONS
73	Ascorbic acid promoted magnetite Fenton degradation of alachlor: Mechanistic insights and kinetic modeling. Applied Catalysis B: Environmental, 2020, 267, 118383.	20.2	113
74	New opportunities for efficient N ₂ fixation by nanosheet photocatalysts. Nanoscale, 2018, 10, 15429-15435.	5.6	111
75	Fe@Fe ₂ O ₃ Coreâ^'Shell Nanowires as an Iron Reagent. 3. Their Combination with CNTs as an Effective Oxygen-Fed Gas Diffusion Electrode in a Neutral Electro-Fenton System. Journal of Physical Chemistry C, 2007, 111, 14799-14803.	3.1	105
76	Selective Synthesis of FeS and FeS ₂ Nanosheet Films on Iron Substrates as Novel Photocathodes for Tandem Dye-Sensitized Solar Cells. Journal of Physical Chemistry C, 2008, 112, 13037-13042.	3.1	105
77	Surface Fe(II)/Fe(III) Cycle Promoted Ultra-Highly Sensitive Electrochemical Sensing of Arsenic(III) with Dumbbell-Like Au/Fe ₃ O ₄ Nanoparticles. Analytical Chemistry, 2018, 90, 4569-4577.	6.5	105
78	Phosphate modification enables high efficiency and electron selectivity of nZVI toward Cr(VI) removal. Applied Catalysis B: Environmental, 2020, 263, 118364.	20.2	97
79	Ascorbic acid enhanced activation of oxygen by ferrous iron: A case of aerobic degradation of rhodamine B. Journal of Hazardous Materials, 2016, 308, 67-74.	12.4	96
80	Insight into the effect of bromine on facet-dependent surface oxygen vacancies construction and stabilization of Bi2MoO6 for efficient photocatalytic NO removal. Applied Catalysis B: Environmental, 2020, 265, 118585.	20.2	96
81	Kirkendall Effect Boosts Phosphorylated nZVI for Efficient Heavy Metal Wastewater Treatment. Angewandte Chemie - International Edition, 2021, 60, 17115-17122.	13.8	95
82	Ultrahigh Peroxymonosulfate Utilization Efficiency over CuO Nanosheets via Heterogeneous Cu(III) Formation and Preferential Electron Transfer during Degradation of Phenols. Environmental Science & Technology, 2022, 56, 8984-8992.	10.0	95
83	Facet-dependent contaminant removal properties of hematite nanocrystals and their environmental implications. Environmental Science: Nano, 2018, 5, 1790-1806.	4.3	93
84	Beyond the Thermal Equilibrium Limit of Ammonia Synthesis with Dual Temperature Zone Catalyst Powered by Solar Light. CheM, 2019, 5, 2702-2717.	11.7	91
85	Hydrogen Spillover to Oxygen Vacancy of TiO _{2–<i>x</i>} H _{<i>y</i>} /Fe: Breaking the Scaling Relationship of Ammonia Synthesis. Journal of the American Chemical Society, 2020, 142, 17403-17412.	13.7	91
86	Visible Light Driven Organic Pollutants Degradation with Hydrothermally Carbonized Sewage Sludge and Oxalate Via Molecular Oxygen Activation. Environmental Science & Technology, 2018, 52, 12656-12666.	10.0	89
87	Photocatalytic NO removal on BiOI surface: The change from nonselective oxidation to selective oxidation. Applied Catalysis B: Environmental, 2015, 168-169, 490-496.	20.2	88
88	Visible light promoted Fe3S4 Fenton oxidation of atrazine. Applied Catalysis B: Environmental, 2020, 277, 119229.	20.2	88
89	In situ growth of epitaxial lead iodide films composed of hexagonal single crystals. Journal of Materials Chemistry, 2005, 15, 4555.	6.7	87
90	Fe@Fe 2 O 3 promoted electrochemical mineralization of atrazine via a triazinon ring opening mechanism. Water Research, 2017, 112, 9-18.	11.3	84

#	Article	IF	CITATIONS
91	Oxygen and Chlorine Dual Vacancies Enable Photocatalytic O ₂ Dissociation into Monatomic Reactive Oxygen on BiOCl for Refractory Aromatic Pollutant Removal. Environmental Science & Technology, 2022, 56, 3587-3595.	10.0	79
92	Ultrasensitive photoelectrochemical determination of chromium(VI) in water samples by ion-imprinted/formate anion-incorporated graphitic carbon nitride nanostructured hybrid. Journal of Hazardous Materials, 2016, 312, 106-113.	12.4	78
93	Rare earth La single atoms supported MoO3-x for efficient photocatalytic nitrogen fixation. Applied Catalysis B: Environmental, 2022, 301, 120766.	20.2	76
94	Atomic‣ayered Cu ₅ Nanoclusters on FeS ₂ with Dual Catalytic Sites for Efficient and Selective H ₂ O ₂ Activation. Angewandte Chemie - International Edition, 2022, 61, .	13.8	75
95	A highly sensitive photoelectrochemical detection of perfluorooctanic acid with molecularly imprined polymer-functionalized nanoarchitectured hybrid of Agl–BiOI composite. Biosensors and Bioelectronics, 2015, 73, 256-263.	10.1	74
96	Enhanced photocatalytic degradation of perfluorooctanoic acid using carbon-modified bismuth phosphate composite: Effectiveness, material synergy and roles of carbon. Chemical Engineering Journal, 2020, 395, 124991.	12.7	74
97	Efficient Visible Light-Driven Photocatalytic Degradation of Pentachlorophenol with Bi ₂ O ₃ /TiO _{2–<i>x</i>} B _{<i>x</i>} . Journal of Physical Chemistry C, 2012, 116, 17118-17123.	3.1	73
98	Photochemical behavior of ferrihydrite-oxalate system: Interfacial reaction mechanism and charge transfer process. Water Research, 2019, 159, 10-19.	11.3	73
99	Diffusionâ€Controlled Zâ€Schemeâ€Steered Charge Separation across PDI/BiOI Heterointerface for Ultraviolet, Visible, and Infrared Lightâ€Driven Photocatalysis. Advanced Functional Materials, 2021, 31, 2102315.	14.9	73
100	Enhanced Cr(VI) removal of zero-valent iron with high proton conductive FeC2O4·2H2O shell. Chemical Engineering Journal, 2020, 389, 124414.	12.7	72
101	Interfacial Charging–Decharging Strategy for Efficient and Selective Aerobic NO Oxidation on Oxygen Vacancy. Environmental Science & Technology, 2019, 53, 6964-6971.	10.0	70
102	Molecularly imprinted ultrathin graphitic carbon nitride nanosheets–Based electrochemiluminescence sensing probe for sensitive detection of perfluorooctanoic acid. Analytica Chimica Acta, 2015, 896, 68-77.	5.4	69
103	Dual-site activation enhanced photocatalytic removal of no with Au/CeO2. Chemical Engineering Journal, 2020, 386, 124047.	12.7	69
104	Rapid Aerobic Inactivation and Facile Removal of <i>Escherichia coli</i> with Amorphous Zero-Valent Iron Microspheres: Indispensable Roles of Reactive Oxygen Species and Iron Corrosion Products. Environmental Science & Technology, 2019, 53, 3707-3717.	10.0	67
105	Structural dependent Cr(VI) adsorption and reduction of biochar: hydrochar versus pyrochar. Science of the Total Environment, 2021, 783, 147084.	8.0	67
106	Neighboring sp-Hybridized Carbon Participated Molecular Oxygen Activation on the Interface of Sub-nanocluster CuO/Graphdiyne. Journal of the American Chemical Society, 2022, 144, 4942-4951.	13.7	67
107	Surface hydrogen bond network spatially confined BiOCl oxygen vacancy for photocatalysis. Science Bulletin, 2020, 65, 1916-1923.	9.0	61
108	Ascorbate Induced Facet Dependent Reductive Dissolution of Hematite Nanocrystals. Journal of Physical Chemistry C, 2017, 121, 1113-1121.	3.1	60

#	Article	IF	CITATIONS
109	Hexavalent chromium removal by a new composite system of dissimilatory iron reduction bacteria Aeromonas hydrophila and nanoscale zero-valent iron. Chemical Engineering Journal, 2019, 362, 63-70.	12.7	60
110	Pyrite enables persulfate activation for efficient atrazine degradation. Chemosphere, 2020, 244, 125568.	8.2	60
111	Enhanced adsorption and photocatalytic degradation of perfluorooctanoic acid in water using iron (hydr)oxides/carbon sphere composite. Chemical Engineering Journal, 2020, 388, 124230.	12.7	60
112	SnO2@C core-shell spheres: synthesis, characterization, and performance in reversible Li-ion storage. Journal of Materials Science, 2008, 43, 2778-2784.	3.7	59
113	Enhanced aerobic degradation of 4-chlorophenol with iron-nickel nanoparticles. Applied Surface Science, 2017, 393, 316-324.	6.1	59
114	Durch Sauerstoffâ€Leerstellen vermittelte Photokatalyse mit BiOCl: Reaktivitä Selektivitäund Ausblick. Angewandte Chemie, 2018, 130, 128-145.	2.0	59
115	Ferrous–tetrapolyphosphate complex induced dioxygen activation for toxic organic pollutants degradation. Separation and Purification Technology, 2013, 120, 148-155.	7.9	58
116	Adsorption and reduction of roxarsone on magnetic greigite (Fe3S4): Indispensable role of structural sulfide. Chemical Engineering Journal, 2017, 330, 1232-1239.	12.7	57
117	Mn2+ promoted Cr(VI) reduction with oxalic acid: The indispensable role of In-situ generated Mn3+. Journal of Hazardous Materials, 2018, 343, 356-363.	12.4	57
118	Controlled Hydrothermal Synthesis and Growth Mechanism of Various Nanostructured Films of Copper and Silver Tellurides. Chemistry - A European Journal, 2006, 12, 4185-4190.	3.3	55
119	Photocatalytic performance of different exposed crystal facets of BiOCl. Current Opinion in Green and Sustainable Chemistry, 2017, 6, 48-56.	5.9	55
120	Anoxic and oxic removal of humic acids with Fe@Fe2O3 core–shell nanowires: A comparative study. Water Research, 2014, 52, 92-100.	11.3	53
121	Highly efficient electrochemical conversion of CO ₂ and NaCl to CO and NaClO. Green Chemistry, 2019, 21, 3256-3262.	9.0	52
122	Persulfate activation induced by ascorbic acid for efficient organic pollutants oxidation. Chemical Engineering Journal, 2020, 382, 122355.	12.7	52
123	Elucidating the Nature of the Cu(I) Active Site in CuO/TiO ₂ for Excellent Low-Temperature CO Oxidation. ACS Applied Materials & Interfaces, 2020, 12, 7091-7101.	8.0	51
124	Vacancy-Rich and Porous NiFe-Layered Double Hydroxide Ultrathin Nanosheets for Efficient Photocatalytic NO Oxidation and Storage. Environmental Science & Technology, 2022, 56, 1771-1779.	10.0	50
125	Sulfur vacancy promoted peroxidase-like activity of magnetic greigite (Fe3S4) for colorimetric detection of serum glucose. Analytica Chimica Acta, 2020, 1127, 246-255.	5.4	49
126	Ascorbate guided conversion of hydrogen peroxide to hydroxyl radical on goethite. Applied Catalysis B: Environmental, 2021, 282, 119558.	20.2	48

#	Article	IF	CITATIONS
127	Modulating Oxygen Reduction Behaviors on Nickel Single-Atom Catalysts to Probe the Electrochemiluminescence Mechanism at the Atomic Level. Analytical Chemistry, 2021, 93, 8663-8670.	6.5	48
128	Ascorbic acid induced atrazine degradation. Journal of Hazardous Materials, 2017, 327, 71-78.	12.4	47
129	Oxalate Modification Dramatically Promoted Cr(VI) Removal with Zero-Valent Iron. ACS ES&T Water, 2021, 1, 2109-2118.	4.6	47
130	Solar-driven efficient methane catalytic oxidation over epitaxial ZnO/La0.8Sr0.2CoO3 heterojunctions. Applied Catalysis B: Environmental, 2020, 265, 118469.	20.2	44
131	Kirkendall Effect Boosts Phosphorylated nZVI for Efficient Heavy Metal Wastewater Treatment. Angewandte Chemie, 2021, 133, 17252-17259.	2.0	44
132	Electrospun template directed molecularly imprinted nanofibers incorporated with BiOI nanoflake arrays as photoactive electrode for photoelectrochemical detection of triphenyl phosphate. Biosensors and Bioelectronics, 2017, 92, 61-67.	10.1	43
133	Rapid photochemical decomposition of perfluorooctanoic acid mediated by a comprehensive effect of nitrogen dioxide radicals and Fe3+/Fe2+ redox cycle. Journal of Hazardous Materials, 2020, 388, 121730.	12.4	43
134	Fabrication of hierarchical porous iron oxide films utilizing the Kirkendall effect. Chemical Communications, 2005, , 2683.	4.1	42
135	Strained Zeroâ€Valent Iron for Highly Efficient Heavy Metal Removal. Advanced Functional Materials, 2022, 32, .	14.9	42
136	Efficient removal of bromate with core-shell Fe@Fe2O3 nanowires. Chemical Engineering Journal, 2017, 308, 880-888.	12.7	41
137	Dechlorination-Hydroxylation of Atrazine to Hydroxyatrazine with Thiosulfate: A Detoxification Strategy in Seconds. Environmental Science & amp; Technology, 2019, 53, 3208-3216.	10.0	41
138	Amorphization enables highly efficient anaerobic thiamphenicol reduction by zero-valent iron. Applied Catalysis B: Environmental, 2020, 264, 118550.	20.2	41
139	Electrochemical Synthesis of Nanostructured Palladium of Different Morphology Directly on Gold Substrate through a Cyclic Deposition/Dissolution Route. Journal of Physical Chemistry C, 2009, 113, 7200-7206.	3.1	39
140	Fenton oxidation of organic contaminants with aquifer sediment activated by ascorbic acid. Chemical Engineering Journal, 2018, 348, 255-262.	12.7	39
141	Simulated solar light driven roxarsone degradation and arsenic immobilization with hematite and oxalate. Chemical Engineering Journal, 2020, 384, 123254.	12.7	39
142	Well-defined Co–Pt–OH as "electronic pump―on Co-LDH nanocages for enhanced oxygen evolution reaction. Applied Catalysis B: Environmental, 2020, 269, 118782.	20.2	38
143	Photothermal reverse-water-gas-shift over Au/CeO2 with high yield and selectivity in CO2 conversion. Catalysis Communications, 2019, 129, 105724.	3.3	37
144	Low temperature synthesis of Î-Bi2O3 solid spheres and their conversion to hierarchical BiOI nests via the Kirkendall effect. CrystEngComm, 2011, 13, 5460.	2.6	36

#	Article	IF	CITATIONS
145	Defectâ€Engineered Nanozymeâ€Linked Receptors. Small, 2021, 17, e2101907.	10.0	36
146	Sulphur vacancy derived anaerobic hydroxyl radical generation at the pyrite-water interface: Pollutants removal and pyrite self-oxidation behavior. Applied Catalysis B: Environmental, 2021, 290, 120051.	20.2	36
147	Manipulating Excitonic Effects in Layered Bismuth Oxyhalides for Photocatalysis. ACS ES&T Engineering, 2022, 2, 957-974.	7.6	36
148	Ferrous ions promoted aerobic simazine degradation with Fe@Fe2O3 core–shell nanowires. Applied Catalysis B: Environmental, 2014, 150-151, 1-11.	20.2	35
149	Boosted photoelectrochemical immunosensing of metronidazole in tablet using coral-like g-C3N4 nanoarchitectures. Biosensors and Bioelectronics, 2019, 123, 7-13.	10.1	35
150	Surface structure-dependent photocatalytic O ₂ activation for pollutant removal with bismuth oxyhalides. Chemical Communications, 2020, 56, 15282-15296.	4.1	35
151	Environmental photochemistry in hematite-oxalate system: Fe(III)-Oxalate complex photolysis and ROS generation. Applied Catalysis B: Environmental, 2021, 283, 119645.	20.2	34
152	An Electrochemical Strategy for Simultaneous Heavy Metal Complexes Wastewater Treatment and Resource Recovery. Environmental Science & Technology, 2022, 56, 10945-10953.	10.0	33
153	A one-step acidification strategy for sewage sludge dewatering with oxalic acid. Chemosphere, 2020, 238, 124598.	8.2	32
154	High-Throughput Signal-On Photoelectrochemical Immunoassay of Lysozyme Based on Hole-Trapping Triggered by Disintegrating Bioconjugates of Dopamine-Grafted Silica Nanospheres. ACS Sensors, 2018, 3, 1480-1488.	7.8	31
155	Atomic-Scale Tuning of Graphene/Cubic SiC Schottky Junction for Stable Low-Bias Photoelectrochemical Solar-to-Fuel Conversion. ACS Nano, 2020, 14, 4905-4915.	14.6	31
156	The surface hydroxyl and oxygen vacancy dependent Cr(<scp>vi</scp>) adsorption performance of BiOCl. Environmental Science: Nano, 2020, 7, 1454-1463.	4.3	30
157	Highly efficient and selective photoreduction of CO2 to CO with nanosheet g-C3N4 as compared with its bulk counterpart. Environmental Research, 2021, 195, 110880.	7.5	30
158	Microstructure-dependent photoelectrochemical and photocatalytic properties of BiOI. Journal of Nanoparticle Research, 2012, 14, 1.	1.9	29
159	Extraction of endocrine disrupting phenols with iron-ferric oxide core-shell nanowires on graphene oxide nanosheets, followed by their determination by HPLC. Mikrochimica Acta, 2015, 182, 2503-2511.	5.0	29
160	Nitrogen dioxide radicals mediated mineralization of perfluorooctanoic acid in aqueous nitrate solution with UV irradiation. Chemosphere, 2017, 188, 367-374.	8.2	29
161	Simulated solar light driven Fe(III)/Fe(II) redox cycle for roxarsone degradation and simultaneous arsenate immobilization. Journal of Hazardous Materials, 2020, 394, 121635.	12.4	29
162	Disposable photoelectrochemical sensing strip for highly sensitive determination of perfluorooctane sulfonyl fluoride on functionalized screen-printed carbon electrode. Talanta, 2018, 181, 147-153.	5.5	28

#	Article	IF	CITATIONS
163	Smart pH-Regulated Switchable Nanoprobes for Photoelectrochemical Multiplex Detection of Antibiotic Resistance Genes. Analytical Chemistry, 2020, 92, 11476-11483.	6.5	27
164	Efficient removal of PFOA with an In2O3/persulfate system under solar light via the combined process of surface radicals and photogenerated holes. Journal of Hazardous Materials, 2022, 423, 127176.	12.4	26
165	O2 activation and 1O2 generation over phosphate modified BiOCl for efficient photodegradation of organic pollutants. Applied Catalysis B: Environmental, 2022, 314, 121520.	20.2	26
166	Magnetic solid-phase extraction followed by high performance liquid chromatography for determination of hexanal and heptanal in human urine. Analytical Methods, 2011, 3, 1418.	2.7	25
167	Oxygen vacancies promote sulfur species accumulation on TiO2 mineral particles. Applied Catalysis B: Environmental, 2021, 290, 120024.	20.2	25
168	C,N-Codoped InOOH microspheres: one-pot synthesis, growth mechanism and visible light photocatalysis. CrystEngComm, 2013, 15, 721-728.	2.6	24
169	Sulfite promoted photochemical cleavage of s-triazine ring: The case study of atrazine. Chemical Engineering Journal, 2017, 330, 1075-1081.	12.7	24
170	Deposition of Prussian blue on nanoporous gold film electrode and its electrocatalytic reduction of H2O2. Journal of Solid State Electrochemistry, 2008, 12, 1567-1571.	2.5	22
171	Molecular O ₂ Activation over Cu(I)-Mediated C≡N Bond for Low-Temperature CO Oxidation. ACS Applied Materials & Interfaces, 2018, 10, 17167-17174.	8.0	22
172	Ni(II) induced aerobic ring opening degradation of atrazine with core-shell Fe@Fe2O3 nanowires. Chemical Engineering Journal, 2018, 335, 720-727.	12.7	21
173	Bifunctional S, N-Codoped carbon dots-based novel electrochemiluminescent bioassay for ultrasensitive detection of atrazine using activated mesoporous biocarbon as enzyme nanocarriers. Analytica Chimica Acta, 2019, 1073, 45-53.	5.4	20
174	Dual-function surface hydrogen bonds enable robust O ₂ activation for deep photocatalytic toluene oxidation. Catalysis Science and Technology, 2021, 11, 319-331.	4.1	20
175	Azo-Enhanced Raman Scattering for Enhancing the Sensitivity and Tuning the Frequency of Molecular Vibrations. ACS Central Science, 2021, 7, 768-780.	11.3	20
176	Molecular Insights into NO-Promoted Sulfate Formation on Model TiO ₂ Nanoparticles with Different Exposed Facets. Environmental Science & Technology, 2018, 52, 14110-14118.	10.0	19
177	Insights into the facet-dependent adsorption of phenylarsonic acid on hematite nanocrystals. Environmental Science: Nano, 2019, 6, 3280-3291.	4.3	19
178	Molecular-scale structures of uranyl surface complexes on hematite facets. Environmental Science: Nano, 2019, 6, 892-903.	4.3	19
179	One-pot template-free synthesis, formation mechanism, and lithium ions storage property of hollow SnO2 microspheres. Journal of Solid State Electrochemistry, 2010, 14, 931-936.	2.5	18
180	Efficient light-driven CO ₂ hydrogenation on Ru/CeO ₂ catalysts. Catalysis Science and Technology, 2018, 8, 6503-6510.	4.1	18

#	Article	IF	CITATIONS
181	Atomically manipulated proton transfer energizes water oxidation on silicon carbide photoanodes. Journal of Materials Chemistry A, 2018, 6, 24358-24366.	10.3	17
182	Protocatechuic acid promoted catalytic degradation of rhodamine B with Fe@Fe2O3 core-shell nanowires by molecular oxygen activation mechanism. Catalysis Today, 2019, 335, 144-150.	4.4	17
183	Photocatalytic oxidative dehydrogenation of cyclohexane to cyclohexene over oxygen-deficient tungsten trioxide. Applied Catalysis B: Environmental, 2021, 298, 120549.	20.2	16
184	Enhanced Cr(<scp>vi</scp>) immobilization on goethite derived from an extremely acidic environment. Environmental Science: Nano, 2019, 6, 2185-2194.	4.3	15
185	Efficient remediation of pentachlorophenol contaminated soil with tetrapolyphosphate washing and subsequent ZVI/Air treatment. Journal of Hazardous Materials, 2015, 292, 27-33.	12.4	14
186	Molecular Oxygen Activation with Nano Zero-valent Iron for Aerobic Degradation of Organic Contaminants and the Performance Enhancement. Acta Chimica Sinica, 2017, 75, 538.	1.4	14
187	Atomic‣ayered Cu ₅ Nanoclusters on FeS ₂ with Dual Catalytic Sites for Efficient and Selective H ₂ O ₂ Activation. Angewandte Chemie, 2022, 134, .	2.0	13
188	FeC2O4•2H2O enables sustainable conversion of hydrogen peroxide to hydroxyl radical for promoted mineralization and detoxification of sulfadimidine. Journal of Hazardous Materials, 2022, 436, 129049.	12.4	12
189	Fabrication and Excellent Antibacterial Activity of Well-defined CuO/Graphdiyne Nanostructure. Chemical Research in Chinese Universities, 2021, 37, 1341-1347.	2.6	11
190	A controllable reduction-oxidation coupling process for chloronitrobenzenes remediation: From lab to field trial. Water Research, 2022, 218, 118453.	11.3	11
191	Hydroxylamine enables rapid heterogeneous-homogeneous coupled Fenton sulfamethazine degradation on ferric phosphate. Applied Catalysis B: Environmental, 2022, 312, 121410.	20.2	11
192	Transformation of Atrazine to Hydroxyatrazine with Alkali-H ₂ O ₂ Treatment: An Efficient Dechlorination Strategy under Alkaline Conditions. ACS ES&T Water, 2021, 1, 1868-1877.	4.6	9
193	New Strategies for Nitrogen Fixation and Pollution Control. Chinese Journal of Chemistry, 2021, 39, 3199-3210.	4.9	9
194	SO2-enhanced nitrate photolysis on TiO2 minerals: A vital role of photochemically reactive holes. Applied Catalysis B: Environmental, 2022, 308, 121217.	20.2	9
195	Efficient degradation of atrazine through in-situ anchoring NiCo2O4 nanosheets on biochar to activate sulfite under neutral condition. Journal of Environmental Sciences, 2023, 126, 81-94.	6.1	9
196	Microwave-assisted synthesis of various gallium oxyhydroxide nanorods and their controllable conversion into different gallium oxide polymorphs. Journal of Materials Research, 2009, 24, 2268-2275.	2.6	8
197	Fast transformation of roxarsone into toxic arsenic species with ferrous iron and tetrapolyphosphate. Environmental Chemistry Letters, 2019, 17, 1077-1084.	16.2	8
198	Plasmonic O ₂ dissociation and spillover expedite selective oxidation of primary C–H bonds. Chemical Science, 2021, 12, 15308-15317.	7.4	8

#	Article	IF	CITATIONS
199	Oxalate promoted iron dissolution of hematite <i>via</i> proton coupled electron transfer. Environmental Science: Nano, 2022, 9, 1770-1779.	4.3	7
200	Rapid ultrasensitive detection of hexavalent chromium in soil and groundwater by a microProbing imaging platform. Journal of Hazardous Materials, 2022, 433, 128809.	12.4	7
201	Membrane disruption boosts iron overload and endogenous oxidative stress to inactivate Escherichia coli by nanoscale zero-valent iron. Journal of Hazardous Materials, 2022, 435, 128951.	12.4	7
202	Robust and well-controlled TiO ₂ –Al ₂ O ₃ binary nanoarray-integrated ceramic honeycomb for efficient propane combustion. CrystEngComm, 2019, 21, 2727-2735.	2.6	5
203	Copper Ions Promoted Aerobic Atrazine Degradation by Fe@Fe2O3 Nanowires. Acta Chimica Sinica, 2017, 75, 602.	1.4	5
204	Doping iodine in CdS for pure hexagonal phase, narrower band gap, and enhanced photocatalytic activity. Journal of Materials Research, 2011, 26, 710-719.	2.6	4
205	Zero-valent iron coupled calcium hydroxide: A highly efficient strategy for removal and magnetic separation of concentrated fluoride from acidic wastewater. Science of the Total Environment, 2022, 838, 156336.	8.0	4
206	Porous In(OH) x S y hollow nanocubes: low-temperature reaction design, shape evolution, growth mechanism, and photoluminescent property. Journal of Nanoparticle Research, 2011, 13, 4121-4131.	1.9	2
207	Synthesis of deuterium-labeled DL-threo-thiamphenicol. Journal of Radioanalytical and Nuclear Chemistry, 2020, 324, 1463-1467.	1.5	0